PHYSICAL REVIEW A **78**, 062708 (2008)

Two-photon photoassociative spectroscopy of ultracold ^{88}Sr

Y. N. Martinez de Escobar,[1] P. G. Mickelson,[1] P. Pellegrini,[2] S. B. Nagel,[1] A. Traverso,[1] M. Yan,[1] R. Côté,[2] and T. C. Killian[1]

[1]*Department of Physics and Astronomy, Rice University, Houston, Texas, 77251, USA*

[2]*Department of Physics, U-3046, University of Connecticut, Storrs, Connecticut, 06269-3046, USA*

(Received 25 August 2008; published 10 December 2008)

We present results from two-photon photoassociative spectroscopy of the least-bound vibrational level of the $X\,^1\Sigma_g^+$ state of the $^{88}Sr_2$ dimer. Measurement of the binding energy allows us to determine the *s*-wave scattering length $a_{88}=-1.4(6)a_0$. For the intermediate state, we use a bound level on the metastable $^1S_0$-$^3P_1$ potential, which provides large Franck-Condon transition factors and narrow one-photon photoassociative lines that are advantageous for observing quantum-optical effects such as Autler-Townes resonance splittings.

DOI: 10.1103/PhysRevA.78.062708 PACS number(s): 34.20.Cf, 32.80.Wr, 34.50.Rk

I. INTRODUCTION

Precise knowledge of interactions between ultracold atoms has enabled spectacular advances in the production and study of quantum gases [1]. The most accurate tool for determining those interactions is spectroscopy of bound molecular states, such as two-photon photoassociative spectroscopy (PAS) in which two laser fields couple colliding atoms to a weakly bound state of the ground molecular potential via a near-resonant intermediate state (Fig. 1). Two-photon PAS has been used to measure binding energies in Li [2,3], Na [4], K [5], Rb [6], Cs [7], He [8], and Yb [9]. Each of these measurements provides accurate determination of the atomic *s*-wave scattering length (a) and understanding of the path towards quantum degeneracy and behavior of resulting quantum fluids. Here, we report two-photon PAS of ^{88}Sr and determination of a for the ground molecular potential ($X\,^1\Sigma_g^+$). Through mass scaling, we also determine a for all stable-isotope collisional combinations.

Alkaline-earth atoms such as Sr, and atoms with similar electronic configuration, differ significantly from alkali-metal atoms that are typically used in ultracold experiments. They have a closed-shell ground state structure, numerous isotopes including spinless bosons, and metastable triplet levels that lead to novel laser-cooling techniques [10] and interactions [11,12]. They present many new opportunities for the study and application of ultracold atoms, such as optical frequency standards [13], long-coherence-time interferometers [14], and Bose and Fermi quantum degenerate gases and mixtures [15,16]. While the collisional properties of these atoms have been the subject of intense study [17–24], until now precise scattering length values have only been published for Yb [9].

For two-photon PAS of Sr, we utilize an intermediate state that is bound in the 0_u potential that corresponds to the $^1S_0+{}^3P_1$ asymptote at long range. The spin-forbidden $^1S_0$-$^3P_1$ intercombination transition at $\lambda=689$ nm is weakly allowed due to spin-orbit coupling of the $^3P_1$ state with the lowest-lying $^1P_1$ level [25]. PAS involving an intercombination line [17,21,26] transition differs qualitatively from spectroscopy near an electric dipole-allowed transition due to the metastability of the $^3P_1$ state ($\tau=21.5$ μs [21]). This increases the importance of the van der Waals interaction relative to the dipole-dipole term in determining the shape of the excited molecular potential, which makes the ground and excited potentials more similar than in alkali-metal atoms. Resulting Franck-Condon factors for transitions from free-atom to weakly bound excited molecular states are smaller, but overlap integrals between excited and ground molecular states are larger, which has implications for the formation of ground state molecules. It has been predicted that an optical Feshbach resonance induced by a laser tuned near an intercombination transition [27] can change the ground state scattering length with much lower inelastic loss [19] than when using electric dipole-allowed transitions [28,29]. Long coherence times are helpful for observing quantum optical effects, such as Autler-Townes splittings [30] of molecular levels [31–33], which is closely related to creation of an atom pair-molecule dark state [8,34,35] and state-selective production of ultracold ground state molecules [32,36,37].

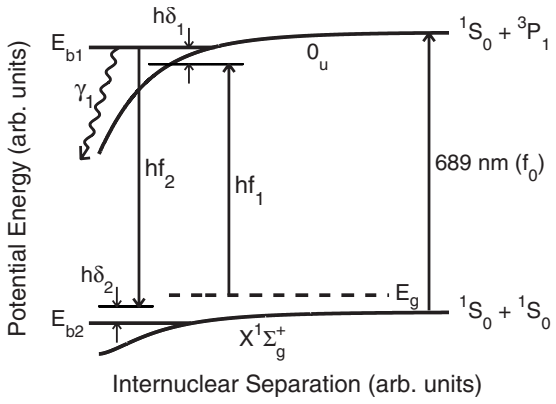

FIG. 1. Two-photon PAS diagram. The energy of two well-separated $^1S_0$ atoms at rest is taken as zero. E_g is the kinetic energy of the colliding atom pair. E_{b_1} is the unperturbed energy of the bound state of the excited molecular potential that is near resonance with the free-bound laser. E_{b_2} (<0) is the unperturbed energy of the bound state of the ground molecular potential. The photon of energy hf_1 is detuned from E_{b1} by $h\delta_1$, while the photon of energy hf_2 is detuned from E_{b2} by $h\delta_2$. The decay rate of b_1 is γ_1. Stark shifts of the levels due to trapping laser fields are neglected in this schematic.

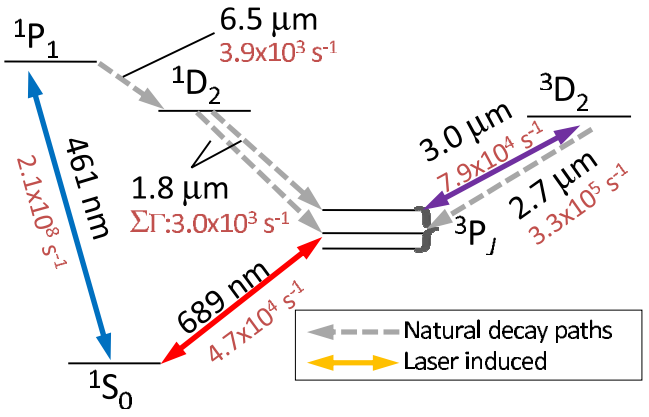

FIG. 2. (Color online) Atomic Sr energy levels involved in the two-photon PAS experiments. Decay rates (s^{-1}) and excitation wavelengths are given for selected transitions. Laser light used for the experiment is indicated by solid lines. Atoms decaying to the $^3P_2$ level may be repumped by 3 μm light.

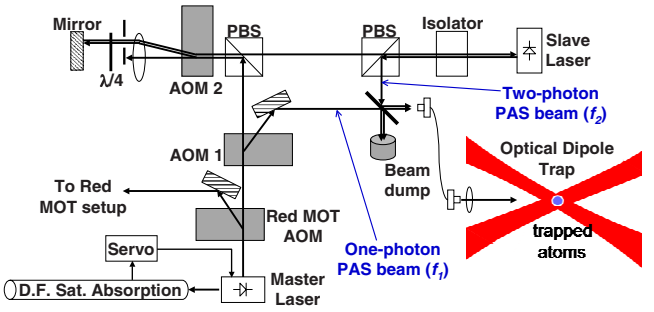

FIG. 3. (Color online) Photoassociation lasers. The master laser that provides light for the intercombination-line MOT is frequency stabilized via saturated absorption spectroscopy to the atomic transition, and it also provides the photoassociation lasers. The one-photon PAS beam, with frequency f_1, is generated directly from the master with an AOM. The two-photon PAS beam, with frequency f_2, is formed by injection-locking a slave diode with a double-passed deflected beam from an AOM in a cat's eye configuration.

II. EXPERIMENTAL SETUP

A. Laser cooling and trapping

To perform two-photon spectroscopy, we start with laser-cooled atoms, and the initial cooling and trapping phases of the experiment are similar to previously published descriptions [12,22,38]. Atoms are trapped in a magneto-optical trap (MOT) operating on the 461 nm $^1S_0$-$^1P_1$ transition (Fig. 2) and cooled to about 2 mK. There is a decay channel from the $^1P_1$ state, through the $^1D_2$ state, to the metastable $^3P_2$ level with a branching ratio of 2×10^{-5}. To increase our sample number, we repump $^3P_2$ atoms by applying a 3 μm laser resonant with the $^3P_2$-$^3D_2$ transition that returns these atoms to the ground state. The repumped sample of atoms contains about 3.5×10^8 atoms.

After this initial MOT stage, the 461 nm light is extinguished and the atom sample is transferred with more than 50% efficiency to a second MOT operating on the $^1S_0$-$^3P_1$ intercombination line [10]. The sample is cooled to 3 μK, producing densities of 10^{12} cm^{-3}. The 689 nm light is provided by a master-slave diode laser system that is frequency-narrowed by servolocking it to a high-finesse optical cavity with the Pound-Drever Hall method to produce a laser linewidth of ~50 kHz. Long-term stability is maintained with a $^1S_0$-$^3P_1$ saturated-absorption cell.

B. Crossed optical dipole trap

To obtain high density and long sample lifetimes for improved two-photon PAS, atoms are transferred to an optical dipole trap (ODT) generated from a 21 W, 1064 nm, linearly polarized, single-transverse-mode fiber laser. The trap is in a crossed-beam configuration, derived from the first order deflection of an acousto-optic modulator (AOM). The beam is focused on the atoms with a minimum e^{-2} intensity radius of $w=75$ μm. It is then reflected back through the chamber to intersect the first beam at 90° and refocused to have the same waist at the atoms. Both beams lie in a plane that is inclined 10.5° from horizontal. The ODT trapping potential is calculated from measured laser beam parameters and the polarizability of the $^1S_0$ state [39]. This allows us to determine the sample density profile from the temperature and number of trapped atoms.

The maximum transfer efficiency observed from intercombination-line MOT to ODT for an optimized overlap time of 80 ms between the two is about 15%. This is limited in large part by inelastic collisions induced by 689 nm light. Atoms are initially loaded with a single-beam ODT power of 5 W, which creates a trap depth of about $U_{\max}/k_B=25$ μK. After the 689 nm light is extinguished, the power is ramped to a final value between 2.5 and 13 W in 20 ms, yielding equilibrium temperatures of between of 3 and 15 μK. Up to 20×10^6 atoms are loaded to yield peak densities on the order of 10^{14} cm^{-3}.

The number of atoms and sample temperature are determined with time-of-flight absorption imaging using the $^1S_0$-$^1P_1$ transition. The lifetime of atoms in the ODT due to collisions with background atoms is about 2 s.

C. Photoassociation

After the atoms have equilibrated in the ODT, the photoassociation lasers are applied (Fig. 1). Laser f_1 is near resonance with a single-photon, free-bound transition to the red of the $^1S_0$-$^3P_1$ atomic transition. For some studies, this is the only laser applied. For two-photon PAS, laser f_2 is near resonance with a transition from the excited molecular bound state to a ground molecular level.

Using acousto-optic modulators, all photoassociation lasers are derived from the master laser that provides the intercombination-line MOT beams (Fig. 3). Both f_1 and f_2 lasers are coupled into the same single-mode optical fiber with the same linear polarization. More than 85% of the intensity of both output beams is linearly polarized in the vertical direction, perpendicular to the ODT laser polarization. These beams are focused to $w=200$ μm at the location of the atom sample, which is substantially larger than the atom cloud. The powers are monitored by a photodiode after the fiber. Alignment of the f_1 and f_2 beams is facilitated by copropagating the beams with 461 nm light aligned on the

ODT atom sample by absorption imaging using an independent CCD camera. Depending on the specific measurement, one of the lasers is scanned and the number of atoms remaining after the photoassociative interaction time is recorded to obtain the loss spectrum.

III. THEORETICAL DESCRIPTION OF PHOTOASSOCIATIVE LOSS

Photoassociation is monitored by measuring the loss of ground-state atoms from the ODT. This loss is described with a local equation for the evolution of the atomic density

$$\dot{n} = -2Kn^2 - \Gamma n, \tag{1}$$

where the laser-frequency dependence of the collision event rate constant K determines the spectrum of the photoassociative loss. The observed PAS spectrum is relatively simple because the bosonic isotopes of strontium lack hyperfine structure. As shown in Fig. 1, ground state $^1S_0$ atoms collide on a single $^1\Sigma_g^+$ potential. Four molecular potentials converge to the $^1S_0+^3P_1$ asymptote [18], but only states of the 0_u and 1_u potentials are optically excited from the $^1\Sigma_g^+$ potential [21]. At the low temperatures of atoms in the ODT, only s-wave collisions occur so only $J=1$ intermediate levels and $J=0$ and 2 final states are populated.

Photoassociative loss can be analyzed with the theory of Bohn and Julienne [40], which yields

$$K = \frac{1}{hQ_T}\int |S(E_g, f_1, f_2, \ldots)|^2 e^{-E_g/k_BT} dE_g, \tag{2}$$

where the partition function is $Q_T=(\frac{2\pi k_B T\mu}{h^2})^{3/2}$ for reduced mass μ. In spite of the low temperature, thermal averaging over the collision energy E_g is necessary because of the narrow linewidth of the transition. $|S|^2$ is the scattering probability for loss and its structure depends upon the loss process that is dominant.

In two-photon spectroscopy of alkali-metal systems, the dominant photoassociative loss process is a collision on the open channel of two ground state atoms (g) with total energy E_g leading to loss-producing decay from the excited state b_1 with rate γ_1 (see Fig. 1). However, in the experiment reported here, b_1 is metastable, and there is a concern that loss from the ground molecular state b_2 may also be important. The complete vanishing of the photoassociative loss when the lasers are on two-photon resonance from $g \rightarrow b_2$ (Secs. V and VI), however, implies that decay from b_2 is negligible for our conditions and loss from b_1 dominates. We can express the scattering probability as

$$|S_{1g}|^2 = \frac{(\delta_1-\delta_2)^2\gamma_1\gamma_s/(2\pi)^2}{\left\{\left[\delta_1-\frac{\delta_2}{2}\right]^2-\frac{1}{4}\left[\delta_2^2+\frac{\Omega_{12}^2}{(2\pi)^2}\right]\right\}^2+\left(\frac{\gamma_1+\gamma_s}{4\pi}\right)^2(\delta_1-\delta_2)^2}. \tag{3}$$

$\gamma_1=2\gamma_{\text{atomic}}$, where γ_{atomic} is the decay rate of the atomic $^3P_1$ level, and $\gamma_s(E_g)$ is the stimulated width of b_1 due to laser-coupling to g,

$$\gamma_s(E_g) = \frac{2\pi V^2|\langle b_1|E_g\rangle|^2}{\hbar}, \tag{4}$$

where we represent g as the energy-normalized colliding state $|E_g\rangle$, leading to the Franck-Condon factor for the free-bound transition $|\langle b_1|E_g\rangle|^2$ and $V=d(\frac{I_1}{2\epsilon_0 c})^{1/2}$ for free-bound laser intensity I_1 and molecular dipole matrix element d. Note that our Ω_{12} is the splitting of the Autler-Townes doublet (Sec. V), which differs from the Bohn-Julienne definition of the molecular Rabi coupling [40].

The thermal energy is much greater than the zero-point energy for trap motion, $T \gg \nu_{\text{trap}}/k_B$, so confinement effects are negligible [21]. We also neglect Doppler shift and photon recoil [17], which is reasonable since $T > T_R$, where the recoil temperature for $\lambda=689$ nm photons is $T_R=h^2/(k_B\lambda^2 m)=460$ nK. We assume the decay products leave the trap, which is a good approximation for the intermediate levels we use, although it is not for the least bound 0_u excited molecular state [21,41].

The energy integral for K [Eq. (2)] is not analytic and must be evaluated numerically. The situation is further complicated by the ODT, which is not at the magic wavelength for one-photon photoassociation (914 nm [21]). The ac Stark shift of the weakly bound ground molecular level (b_2) is approximately equal to the shift of the incoming channel of two free atoms (g) [37,42]. In other words, the polarizability of the ground molecule is about twice that of a single atom. But the ground and excited molecular levels do not experience the same shift. For spectroscopy, we can thus treat the ODT Stark shifts as a position-dependent shift of the intermediate state and define the laser detunings

$$\delta_1 = f_1 - (E_{b_1} - E_g)/h - \chi I_{\text{ODT}}(\vec{r}),$$

$$\delta_2 = f_2 - (E_{b_1} - E_{b_2})/h - \chi I_{\text{ODT}}(\vec{r}), \tag{5}$$

where $I_{\text{ODT}}(\vec{r})$ is the intensity profile of the optical dipole trap and χ can be related to the differences in polarizabilites for $^1S_0$ and $^3P_1$ atoms for 1.06 μm laser light.

This implies that $|S|^2$ and thus K are functions of position, which must be addressed when Eq. (1) is integrated over the

trap volume to calculate the time evolution of the number of trapped atoms

$$N(t) = \frac{N_0 e^{-\Gamma t}}{1 + \frac{2N_0 K_{\rm eff} V_2}{\Gamma V_1^2}(1 - e^{-\Gamma t})}, \tag{6}$$

where N_0 is the number at the beginning of the PAS interaction time. The one-body loss rate Γ is due to background collisions and off-resonant scattering from the PAS lasers. The effective volumes are defined by

$$V_q = \int_V d^3 r e^{-qU(\vec{r})/k_B T}, \tag{7}$$

where $U(r)$ is the trap potential and

$$K_{\rm eff} = \frac{1}{V_2}\int_V d^3 r e^{-2U(\vec{r})/k_B T} \times \frac{1}{hQ_T}\int_0^{U_{\rm max}-U(r)} dE_g |S_{1g}|^2 e^{-E_g/k_B T}. \tag{8}$$

The kinetic energy integral is truncated by the local trap depth $U_{\rm max} - U(r)$. The spatial integrals in Eqs. (7) and (8) extend over the trap volume V in which $U(r) < U_{\rm max}$. Atom temperatures vary by no more than 25% during the interaction time, so assuming a constant sample temperature is reasonable.

The spectrum is sensitive to many atomic and molecular parameters, and multiple types of spectra can be used to determine them. The ultimate goal is an accurate determination of E_{b_2} because the molecular binding energy determines the s-wave scattering length and the underlying potential with high accuracy.

IV. ONE-PHOTON PHOTOASSOCIATION

A. One-photon PAS spectrum

One photon PAS allows us to determine χ, the relative light shift of states on the ground and excited molecular potentials [Eq. (5)] and the stimulated width $\gamma_s(E_g)$ [Eq. (4)]. When $I_2 = 0$ and $\Omega_{12} = 0$ in Eq. (3), we recover the one-photon PAS scattering probability for loss through decay of b_1

$$|S_{1g}|^2 = \frac{\gamma_1 \gamma_s/(2\pi)^2}{\delta_1^2 + \frac{1}{(2\pi)^2}\left(\frac{\gamma_1 + \gamma_s}{2}\right)^2}. \tag{9}$$

The state b_1 is equal to the $J=1$ rotational state of the third-least bound vibrational level of the 0_u potential, with energy $E_{b_1} = E_{3P_1} - h \times 222.161(35)$ MHz [21]. The Condon point for this excitation, where $V_{0_u}(R_c) - V_{1S_0}(R_c) = E_{b_1}$, occurs at $R_c = 75\ a_0$, which is very near the node in the ground state wave function [22,43]. Fitting data of atom number after a given interaction time, $N(t)$, to Eq. (6) yields the collision-event rate constant $K_{\rm eff}$. Figure 4 shows typical spectra for this transition.

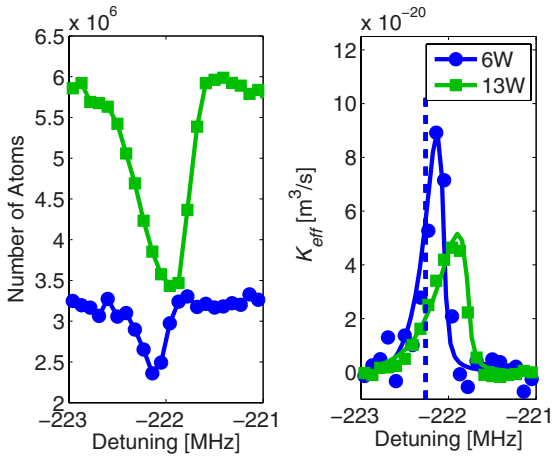

FIG. 4. (Color online) Left: Atom number versus free-bound laser detuning from the one-photon ${}^1S_0$-${}^3P_1$ atomic transition. Spectra shown here are for 6 and 13 W ODT single-beam powers with sample temperatures of 6 and 13 μK, respectively. Right: Collision-event rate constant $K_{\rm eff}$ derived from the atom loss. The ODT at 1064 nm causes an ac Stark shift of the excited molecular state compared to the ground state, which shifts and broadens the line. The solid lines are fits using Eqs. (8) and (9). A peak shift of 480 kHz is measured for a single-beam power of 13 W. The dashed line marks the position of our measured unperturbed resonance frequency at −222.25(15) MHz, which is in reasonable agreement with a previous measurement of −222.161(35) MHz [21].

B. Determining the stimulated width

The area under the one-photon PAS line (Fig. 4) can be related to molecular and experimental parameters through

$$A = \int df K_{\rm eff} = \frac{1}{hQ_T}\int dE_g e^{-E_g/k_B T}\frac{\gamma_s(E_g)\gamma_1}{\gamma_s(E_g) + \gamma_1}. \tag{10}$$

Here, we have neglected truncation of the energy integral, which is a small correction. The Wigner threshold law implies $\gamma_s(E_g) \propto I_1 \sqrt{E_g}$. So for low laser intensity $[\gamma_s(E_g) \ll \gamma_1]$, the expression $A \approx \frac{k_B T}{hQ_T}\langle \gamma_s(E_g)\rangle$ is independent of temperature and linearly dependent on intensity (Fig. 5), where $\langle \cdots \rangle$ refers to a thermal average. The PAS saturation intensity for this transition ($I_{\rm sat,PAS} \propto 1/T^{1/2}$) defined as the intensity for which $\langle \gamma_s(E_g)\rangle = \gamma_1$, is 8 W/cm^2 for $T = 13\ \mu$K. Expressing this in terms of an optical length for the transition $l_{\rm opt} = \frac{\gamma_s(E_g)}{2k_r\gamma_1}$, where $k_r = \sqrt{2\mu E_g}/\hbar$, yields $l_{\rm opt} = 28 a_0$ for $I_1 = 1$ W/cm^2 for this transition.

C. Modeling the spectra and determining the relative ac Stark shift

Numerical integration of Eq. (8) to find $K_{\rm eff}$ using Eq. (9) for the scattering probability allows us to model the one-photon PAS spectra, and the relative light shift parameter [Eq. (5)] can be varied to fit the data (Fig. 4). We find $\chi = 160 \pm 30$ kHz/(100 kW/cm^2), in good agreement with Ref. [39], which yields a peak shift of 480 kHz for our deepest trap. The line shifts to the blue with more ODT laser intensity, showing the polarizability of ${}^3P_1$ atoms is less than the polarizability of ${}^1S_0$ atoms. At higher temperatures, the

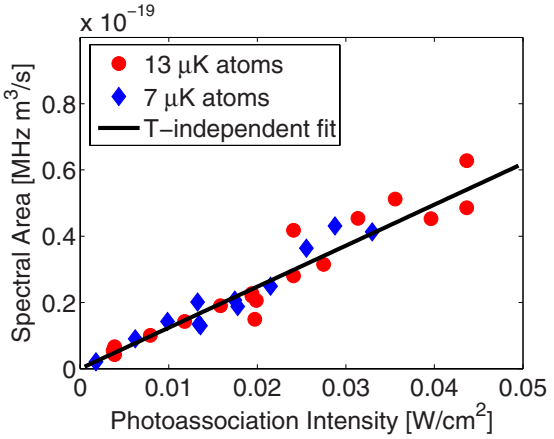

FIG. 5. (Color online) Area under one-photon PAS spectra versus free-bound laser intensity I_1. The area can be related to molecular and experimental parameters to determine the stimulated linewidth $\gamma_s(E_g)$ of the PAS transition due to I_1. For low free-bound laser intensities the area is independent of temperature and linearly dependent on I_1.

line shapes in Fig. 4 possess red tails, which result from the convolution of the Lorentzian spectrum with the Maxwell-Boltzmann distribution of collision energies [17,21].

V. TWO-PHOTON AUTLER TOWNES SPECTRUM

If PAS spectra are recorded in the same fashion as in Sec. IV, except the bound-bound laser is added near resonance ($\delta_2 \approx 0$) with a large intensity I_2, the loss spectrum is modified due to the coupling between b_1 and b_2. This forms a Λ system and the line is split into an Autler-Townes doublet, with splitting given approximately by $\Omega_{12}/2\pi$, where

$$\Omega_{12} = \alpha |\langle b_1 | b_2 \rangle| \gamma_1 \sqrt{\frac{I}{4I_{\text{sat,atom}}}}. \tag{11}$$

The overlap integral is related to the Franck-Condon factor F through $F = |\langle b_1 | b_2 \rangle|^2$. The saturation intensity for the atomic ${}^1S_0$-${}^3P_1$ transition is $I_{\text{sat,atom}} \equiv \pi hc\gamma_{\text{atomic}}/(3\lambda^3) = 3\ \mu\text{W/cm}^2$. The rotational line strength factor, α, accounts for the change in dipole moment from atom to molecule due to symmetry of wave function and projection on a rotating molecular axis [18,20].

Figure 6 shows several Autler-Townes spectra for various intensities I_2 for a ground molecular state (b_2) equal to the $J=0$ rotational state of the least-bound ground vibrational level. This is the $v=62$ level counting from the bottom of the well (see Sec. VII). We find that $\Omega_{12}/2\pi = 1$ MHz for an intensity of 0.35 W/cm^2, which yields $F = 0.28 \pm 0.06$ for $\alpha = \sqrt{2/3}$ [18]. The energy of the ground molecular state E_{b_2} can be found from fits of data in Fig. 6, but it is more accurately found by varying δ_2 with $\delta_1 \approx 0$, as we will discuss in Sec. VI.

The asymmetry in the line strengths in each doublet in Fig. 6 arises from the coupling-laser frequency being slightly off resonance from the Stark-shifted bound-bound transition ($\delta_2 \neq 0$). But δ_2 is small and the scaling with intensity shows

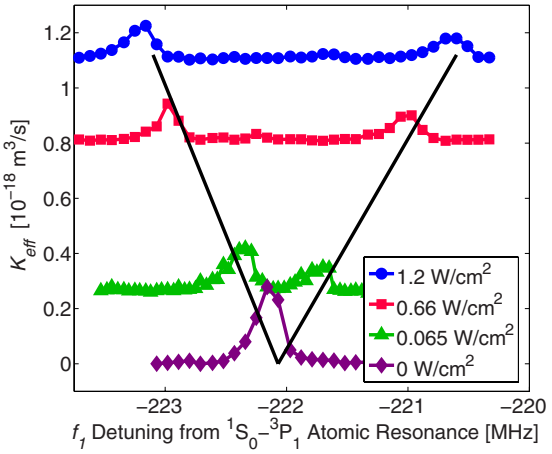

FIG. 6. (Color online) Collision-event rate constant K_{eff} versus free-bound laser detuning from ${}^1S_0$-${}^3P_1$ atomic resonance for different bound-bound laser intensities. These Autler-Townes doublets are measured with the bound-bound laser frequency fixed such that $\delta_2 \approx 0$ while scanning f_1. The splitting of the spectra is given by the Rabi frequency $\Omega_{12}/2\pi$ and varies as $\sqrt{I_2}$ (shown by the lines; spectra offset is proportional to $\sqrt{I_2}$), where the bound-bound laser intensity I_2 is indicated in the legend. The asymmetry in the line shapes arises from the bound-bound laser frequency being slightly off resonance from the bound-bound transition. The free-bound intensity I_1 is constant for all four spectra at 0.05 W/cm^2. The sample temperature is 8 μK.

that the Autler-Townes splitting varies as $\sqrt{I_2}$ as expected.

These spectra show the potential of the system for quantum optics and ultracold molecule formation. The condition of no PAS loss when both lasers are on resonance has also been called a dark resonance [8], or an atom pair-molecule dark state [34] because the system has been put in an atom pair-molecule superposition state with vanishing excitation rate to b_1. Such a state has also been proposed as a vehicle for creating large numbers of ground state molecules using STIRAP [44]. The level of suppression near $\delta_1 = 0$ shows the coherence of this superposition state in these experiments. It is noteworthy that the doublet is split by many linewidths even with moderate coupling-laser intensity because of the intrinsically narrow spectrum of intercombination-line PAS.

VI. TWO-PHOTON SUPPRESSION OF PHOTOASSOCIATION

For determining the binding energy of molecular levels of the ground state potential, we hold the frequency of the free-bound laser fixed close to the one-photon resonance $\delta_1 \simeq 0$ and scan δ_2. When $\delta_2 - \delta_1 = 0$, the system is in two-photon resonance from state g to b_2, and one-photon photoassociative loss is suppressed due to quantum interference. At this point, $f_1 - f_2 = (E_{b2} - E_g)/h$, so the spectrum allows accurate determination of E_{b_2}. An average over E_g is necessary in order to properly account for thermal shifts of the resonance.

Figure 7 shows a series of spectra taken at various bound-bound intensities for b_2 equal to the $J=0$, $v=62$ state. Detuning of the free-bound laser frequency (f_1) from the free-bound resonance, which depends on the ODT light shift (χ)

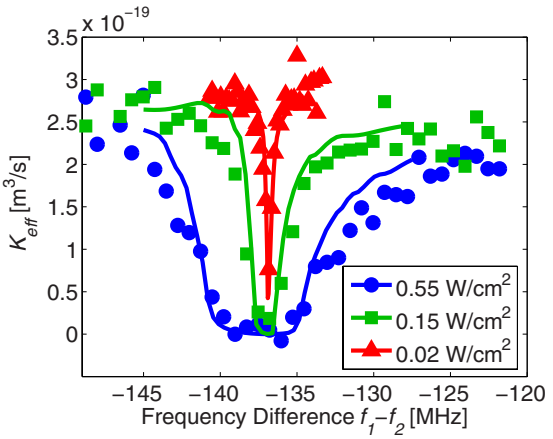

FIG. 7. (Color online) Collision-event rate constant K_{eff} versus frequency difference between free-bound and bound-bound lasers for spectroscopy of the $J=0$, $v=62$ level of the $X\ ^1\Sigma_g^+$ potential. The free-bound laser frequency is fixed close to the one-photon PAS resonance and the intensity is $I_1=0.05$ W/cm^2. The bound-bound laser frequency is scanned, and its intensity is indicated in the legend. On two-photon resonance, PAS loss is suppressed due to quantum interference. The solid lines are fits using Eqs. (8) and (3), which yield $E_{b2}/h=-136.7(2)$ MHz. The atom temperature is 8 μK.

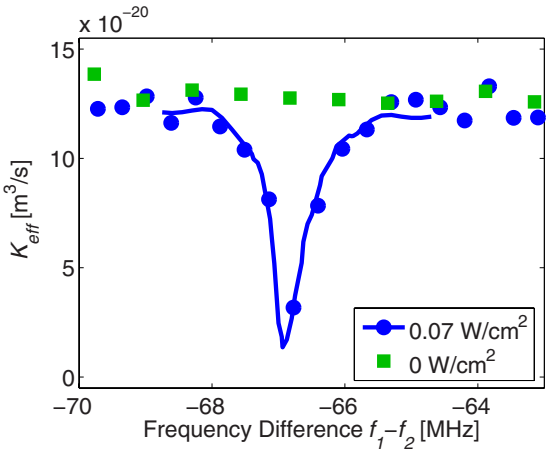

FIG. 8. (Color online) PAS suppression spectra for the $J=2$, $v=62$ level of the ground molecular potential, as described in Fig. 7. The sample temperature is 9 μK. The free-bound laser intensity is $I_1=0.04$ W/cm^2, and the bound-bound intensity is indicated in the legend. The solid line is a fit using Eqs. (8) and (3), which yields $E_{b2}/h=-66.6(2)$ MHz.

and collision energy (E_g), causes slight asymmetry in the lines and broadening, but this shape is reproduced with our model for K_{eff} [Eq. (8)] using parameters independently determined in previous sections. Since the initial and final states experience roughly equal light shifts due to the trapping laser, the ODT ac Stark shifts do not shift the resonance. No significant shift of the binding energy with laser power was observed, and we place an upper limit of 100 kHz for our highest intensity $I_2=0.55$ W/cm^2. We have also measured the binding energy of the $J=2$, $v=62$ state (Table I) and a typical spectrum is shown in Fig. 8.

VII. DETERMINATION OF THE SCATTERING LENGTH

Binding energy measurements can be used to accurately determine the s-wave scattering length for the $X\ ^1\Sigma_g^+$ ground electronic molecular potential and to obtain information on the van der Waals coefficients C_n. For our analysis, the inner part (internuclear spacing $R<20.8a_0$) of the potential is described with a recently published energy curve [45] derived from the Fourier-transform spectrum of Sr_2 and additional information on the zero-energy ground-state scattering wave function from PAS [22,43]. A multipolar van der Waals expansion in C_n/R^n [46] is used to represent the potential at longer range ($R>22.7a_0$), and the gap between the two regions is bridged with a spline interpolation to insure a smooth connection. The wave functions are calculated using a full quantum calculation [22]. With this input on the potentials, the vibrational assignment of the observed ground-state levels is unambiguous.

TABLE I. Observed ground molecular levels and experimental and theoretical level energies in frequency units (E_{b2}/h).

Isotope	v	J	Exp. (MHz)	Theory (MHz)	Diff. (MHz)
88	62	0	−136.7(2)	−136.7	0.0
88	62	2	−66.6(2)	−66.5	−0.1

As was the case in the analysis of Ref. [45], we do not have enough information to independently determine all the van der Waals coefficients, and improve on the precise relativistic many-body calculation of Ref. [46], which gave $C_6=3103(7)$ a.u., $C_8=3.792(8)\times10^5$ a.u., and $C_{10}=4.215\times10^7$ a.u. The last bound level ($v=62, J=0$) is very extended, with its outer turning point at roughly $R\sim100a_0$. At this point, the leading contribution to the dispersion energy $-C_6/R^6-C_8/R^8-C_{10}/R^{10}$ arises from the C_6 term. In fact, using the values of C_n above, the C_8 contribution is only 1.22% of that of C_6, while the C_{10} contribution accounts for only 0.02%. At a shorter distance $R\sim20a_0$, similar to the maximum separation of states measured in Ref. [45], these contributions are roughly 30.5 and 8.5%, respectively. In Ref. [45], the precise theoretical values of [46] for C_6 and C_8 were used to fit the value of C_{10}, since the energy levels ($v=0-50$) were more deeply bound and corresponded to shorter range than our levels ($v=62, J=0$ and 2). We note that less precise values of C_6 and C_8 from Ref. [47] were also considered in Ref. [45].

If we use C_6 as a fit parameter to match the binding energy of the $J=0$, $v=62$ state, assuming C_8 and C_{10} from [46], the best fit value is $C_6=3151(1)$ a.u. where the quoted uncertainty only reflects uncertainty in the measured binding energy (see Table I). The resulting ^{88}Sr $X\ ^1\Sigma_g^+$ s-wave scattering length is $a=-2.0(2)a_0$, where the uncertainty also only reflects uncertainty in the measured binding energy. If we use the value of $C_{10}=6.60\times10^7$ a.u. from Ref. [45] instead, we find $C_6=3116.0(5)$ a.u., in reasonable agreement with Ref. [46]. The resulting scattering length is $a=-1.2(2)a_0$. If instead, we take C_6 and C_8 from Ref. [46], and fit C_{10}, as was done in Ref. [45], we find $C_{10}=7.488\times10^7$ a.u. and $a=-0.9(2)a_0$ (again, with the uncertainties reflecting the uncertainty in the measured binding energy).

TABLE II. Published values of scattering lengths given in units of $a_0=0.053$ nm.

Isotopes	2-phot. PAS (this study) a	Fourier-transform [45] a	1-phot. PAS [22] a	1-phot. PAS [43] a	Thermalization [48] $\lvert a\rvert$
88-88	−1.4(6)	0(5)	10^{+3}_{-11}	-40^{+40}_{-100}	21^{+3}_{-4}
87-87	96.2(1)	97(2)			
86-86	823(24)	1050(380)	1000^{+1300}_{-400}		430^{+80}_{-90}
84-84	122.7(3)	124(3)			
88-87	55.0(2)	56(2)			
88-86	97.4(1)	99(2)			110^{+10}_{-20}
88-84	1790(130)	>1170 or <−1900			
87-86	162.5(5)	165.5(5.5)			
87-84	−56(1)	−55(10)			
86-84	31.9(3)	33(3)			

It is difficult to assess the uncertainties in a related to these coefficients. The most conservative assessment encompasses the full range of values quoted here; $a=-1.4(6)$ and $C_6=3130(20)$ a.u. The uncertainties in C_6 and C_8 quoted in Ref. [46] are quite small, however, and no uncertainty is quoted for C_{10}. So that might give more credence to the results for C_6 and C_8 from Ref. [46] and the resulting fit $C_{10}=7.488\times10^7$ a.u., which corresponds to the higher ends of the ranges of values for a in Table II. Mass-scaling can be used to determine the scattering lengths for all stable-isotope collisional combinations from this information about the potential (Table II).

We note that the rotational energy takes the form $H_{\rm rot}=B(R)J(J+1)$ where $B(R)=\hbar^2/(2\mu R^2)$ is the rotational constant for separation R and reduced mass μ. The rotational constant for $v=62$ calculated using this potential yields a binding energy of −66.5 MHz for the $J=2$, $v=62$ state (Table I), well within the measurement uncertainty. We also found that this quantity does not significantly constrain the C_n coefficients.

According to the Wigner threshold law [49], the elastic cross section for collisions between neutral particles approaches a constant as the collision energy goes to zero. Most experiments with ultracold distinguishable particles or indistinguishable bosons reach this limit where the cross section is well described by the $l=0$ partial wave, and its energy dependence can be neglected [50]. However, this is not the case when there is a low-energy scattering resonance or when the scattering length is very small. Figure 9 demonstrates that ^{88}Sr-^{88}Sr and ^{86}Sr-^{86}Sr collision cross-sections vary significantly with collision energy, even at energies below 1 μK.

These results can be compared to previous thermalization studies of Sr collisional properties [48] as shown in Fig. 9. A complete simulation of the collision dynamics, including the energy-dependent cross section, is beyond the scope of this paper. But one expects that collision energies with larger cross-section will contribute more to thermalization, increasing the apparent ^{88}Sr-^{88}Sr cross section and decreasing the value for ^{86}Sr-^{86}Sr collisions. So the agreement is reasonable.

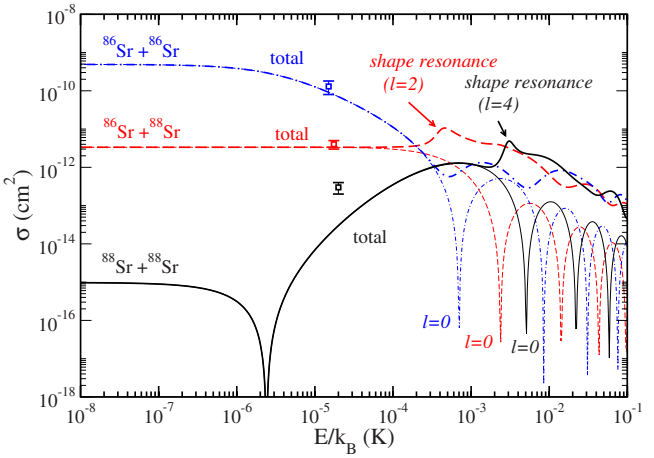

FIG. 9. (Color online) Dependence of elastic-scattering cross sections on collision energy (E) for selected Sr isotopes. The thick lines are cross sections including partial waves up to $l=4$. Shape resonances are indicated. Thin lines indicate cross section contributions from $l=0$ only. For the plot, a potential is used that gives $a_{88-88}=-1.2a_0$ at $E=0$. The cross sections are given by the usual expressions $\sigma=(8\pi/k^2)\Sigma_{l=0,2,\ldots}^{\infty}(2l+1)\sin^2\delta_l(k)\overset{k\to0}{\to}8\pi a^2$ for identical bosons and $\sigma=(4\pi/k^2)\Sigma_{l=0}^{\infty}(2l+1)\sin^2\delta_l(k)\overset{k\to0}{\to}4\pi a^2$ for distinguishable atoms. The phase shift, $\delta_{l=0}(k)$, depends on $k=\sqrt{2\mu E}/\hbar$ and is related to the scattering length a and effective range r_e at low k by $k\cot\delta_{l=0}(k)=-\frac{1}{a}+\frac{1}{2}r_e k^2$. The data symbols are cross section measurements from thermalization experiments [48], and the respective collision energies are set to $E=k_BT$, where T is the sample temperature.

VIII. CONCLUSION

Using two-photon photoassociative spectroscopy, we have measured the binding energy of the $J=0$ and $J=2$ rotational levels of the $v=62$ vibrational state of the $X\,^1\Sigma_g^+$ potential of $^{88}Sr_2$. This is the least-bound ground vibrational level. Combined with an accurate short range potential [45] and calculated van der Waals coefficients [46], the measurement allows an accurate determination of a for ^{88}Sr-^{88}Sr interactions. Through mass scaling, we determine the scattering lengths for all other isotopic combinations. These measurements provide confirmation of atomic structure calculations for alkaline-earth atoms and will provide valuable input for future experiments with ultracold strontium.

ACKNOWLEDGMENTS

We thank P. Julienne, R. Hulet, and E. Tiemann for helpful discussions. P.P. was supported by the U.S. Department of Energy, Office of Basic Energy Sciences. This work was supported by the Welch Foundation (Grant No. C-1579), National Science Foundation (Grants No. PHY-0555639 and No. PHY 0653449), and the Keck Foundation.

[1] K. M. Jones, E. Tiesinga, P. D. Lett, and P. S. Julienne, Rev. Mod. Phys. **78**, 483 (2006).
[2] E. R. I. Abraham, W. I. McAlexander, J. M. Gerton, R. G. Hulet, R. Côté, and A. Dalgarno, Phys. Rev. A **55**, R3299 (1997).
[3] E. R. I. Abraham, W. I. McAlexander, C. A. Sackett, and R. G. Hulet, Phys. Rev. Lett. **74**, 1315 (1995).
[4] F. A. van Abeelen and B. J. Verhaar, Phys. Rev. A **59**, 578 (1999).
[5] H. Wang *et al.*, Phys. Rev. A **62**, 052704 (2000).
[6] C. C. Tsai, R. S. Freeland, J. M. Vogels, H. M. J. M. Boesten, B. J. Verhaar, and D. J. Heinzen, Phys. Rev. Lett. **79**, 1245 (1997).
[7] N. Vanhaecke, C. Lisdat, B. T'Jampens, D. Comparat, A. Crubellier, and P. Pillet, Eur. Phys. J. D **28**, 351 (2004).
[8] S. Moal, M. Portier, J. Kim, J. Dugué, U. D. Rapol, M. Leduc, and C. Cohen-Tannoudji, Phys. Rev. Lett. **96**, 023203 (2006).
[9] M. Kitagawa, K. Enomoto, K. Kasa, Y. Takahashi, R. Ciuryło, P. Naidon, and P. S. Julienne, Phys. Rev. A **77**, 012719 (2008).
[10] H. Katori, T. Ido, Y. Isoya, and M. Kuwata-Gonokami, Phys. Rev. Lett. **82**, 1116 (1999).
[11] V. Kokoouline, R. Santra, and C. H. Greene, Phys. Rev. Lett. **90**, 253201 (2003).
[12] S. B. Nagel, C. E. Simien, S. Laha, P. Gupta, V. S. Ashoka, and T. C. Killian, Phys. Rev. A **67**, 011401(R) (2003).
[13] A. D. Ludlow *et al.*, Science **319**, 1805 (2008).
[14] G. Ferrari, N. Poli, F. Sorrentino, and G. M. Tino, Phys. Rev. Lett. **97**, 060402 (2006).
[15] Y. Takasu, K. Maki, K. Komori, T. Takano, K. Honda, M. Kumakura, T. Yabuzaki, and Y. Takahashi, Phys. Rev. Lett. **91**, 040404 (2003).
[16] T. Fukuhara, Y. Takasu, M. Kumakura, and Y. Takahashi, Phys. Rev. Lett. **98**, 030401 (2007).
[17] R. Ciuryło, E. Tiesinga, S. Kotochigova, and P. S. Julienne, Phys. Rev. A **70**, 062710 (2004).
[18] M. Machholm, P. S. Julienne, and K.-A. Suominen, Phys. Rev. A **64**, 033425 (2001).
[19] R. Ciuryło, E. Tiesinga, and P. S. Julienne, Phys. Rev. A **71**, 030701(R) (2005).
[20] P. Naidon and P. S. Julienne, Phys. Rev. A **74**, 062713 (2006).
[21] T. Zelevinsky, M. M. Boyd, A. D. Ludlow, T. Ido, J. Ye, R. Ciuryło, P. Naidon, and P. S. Julienne, Phys. Rev. Lett. **96**, 203201 (2006).
[22] P. G. Mickelson, Y. N. Martinez, A. D. Saenz, S. B. Nagel, Y. C. Chen, T. C. Killian, P. Pellegrini, and R. Cote, Phys. Rev. Lett. **95**, 223002 (2005).
[23] O. Allard, C. Samuelis, A. Pashov, H. Knockel, and E. Tiemann, Eur. Phys. J. D **26**, 155 (2003).
[24] C. Degenhardt, T. Binnewies, G. Wilpers, U. Sterr, F. Riehle, C. Lisdat, and E. Tiemann, Phys. Rev. A **67**, 043408 (2003).
[25] R. Santra, K. V. Christ, and C. H. Greene, Phys. Rev. A **69**, 042510 (2004).
[26] S. Tojo, M. Kitagawa, K. Enomoto, Y. Kato, Y. Takasu, M. Kumakura, and Y. Takahashi, Phys. Rev. Lett. **96**, 153201 (2006).
[27] P. O. Fedichev, Y. Kagan, G. V. Shlyapnikov, and J. T. M. Walraven, Phys. Rev. Lett. **77**, 2913 (1996).
[28] F. K. Fatemi, K. M. Jones, and P. D. Lett, Phys. Rev. Lett. **85**, 4462 (2000).
[29] M. Theis, G. Thalhammer, K. Winkler, M. Hellwig, G. Ruff, R. Grimm, and J. H. Denschlag, Phys. Rev. Lett. **93**, 123001 (2004).
[30] S. H. Autler and C. H. Townes, Phys. Rev. **100**, 703 (1955).
[31] U. Schloder, T. Deuschle, C. Silber, and C. Zimmermann, Phys. Rev. A **68**, 051403(R) (2003).
[32] B. Laburthe Tolra, C. Drag, and P. Pillet, Phys. Rev. A **64**, 061401(R) (2001).
[33] R. Dumke, J. D. Weinstein, M. Johanning, K. M. Jones, and P. D. Lett, Phys. Rev. A **72**, 041801 (2005).
[34] K. Winkler, G. Thalhammer, M. Theis, H. Ritsch, R. Grimm, and J. H. Denschlag, Phys. Rev. Lett. **95**, 063202 (2005).
[35] C. Lisdat, N. Vanhaecke, D. Comparat, and P. Pillet, Eur. Phys. J. D **21**, 299 (2002).
[36] R. Wynar, R. S. Freeland, D. J. Han, C. Ryu, and D. J. Heinzen, Science **287**, 1016 (2000).
[37] T. Rom, T. Best, O. Mandel, A. Widera, M. Greiner, T. W. Hansch, and I. Bloch, Phys. Rev. Lett. **93**, 073002 (2004).
[38] S. B. Nagel, P. G. Mickelson, A. D. Saenz, Y. N. Martinez, Y. C. Chen, T. C. Killian, P. Pellegrini, and R. Côté, Phys. Rev. Lett. **94**, 083004 (2005).
[39] J. Ye, H. J. Kimble, and H. Katori, Science **320**, 1734 (2008).
[40] J. L. Bohn and P. S. Julienne, Phys. Rev. A **54**, R4637 (1996).
[41] P. Julienne (private communication).
[42] L. B. Ratcliff, J. L. Fish, and D. D. Konowalow, J. Mol. Spectrosc. **122**, 293 (1987).
[43] M. Yasuda, T. Kishimoto, M. Takamoto, and H. Katori, Phys. Rev. A **73**, 011403(R) (2006).
[44] M. Mackie, R. Kowalski, and J. Javanainen, Phys. Rev. Lett. **84**, 3803 (2000).
[45] A. Stein, H. Knöckel, and E. Tiemann, e-print arXiv:0807.4664.
[46] S. G. Porsev and A. Derevianko, J. Exp. Theor. Phys. **102**, 195 (2006).
[47] J. Mitroy and M. W. J. Bromley, Phys. Rev. A **68**, 052714 (2003).
[48] G. Ferrari, R. E. Drullinger, N. Poli, F. Sorrentino, and G. M. Tino, Phys. Rev. A **73**, 023408 (2006).
[49] E. P. Wigner, Phys. Rev. **73**, 1002 (1948).
[50] P. S. Julienne and F. H. Mies, J. Opt. Soc. Am. B **6**, 2257 (1989).